Acta Geochim (2024) 43:478–488
https://doi.org/10.1007/s11631-024-00675-5

ORIGINAL ARTICLE

In-situ analysis and genetic investigation of Li-bearing minerals in McDermitt clay-type lithium deposit, Nevada, USA

Yi Cui[1,2] · Hanjie Wen[3,4] · Zhengbing Zhou[1,2] · Kunyue Ling[5] · Lin Xu[1,2] · Shirong Liu[6] · Fei Xu[3]

Received: 7 December 2023 / Revised: 16 January 2024 / Accepted: 24 January 2024 / Published online: 1 March 2024

Abstract Clay-type Li deposits are poised to play a pivotal role in addressing the surging global demand for Li. The McDermitt clay-type Li deposit, located in Nevada, is the largest Li deposit in the United States, with Li hosted by a clay-rich sequence of smectite-dominated intervals and illite-dominated intervals, respectively. However, the occurrence of Li and the genesis of Li-bearing minerals within smectite-dominated intervals have not been thoroughly investigated in previous research. Here, we studied the mineralogy, the in-situ Li distribution, and the bonding environments of Li within the smectite intervals using a combination of instrumental techniques including scanning electron microscope, transmission electron microscope, time-of-flight secondary ion mass spectrometry, and nuclear magnetic resonance. Our results indicate that the smectite exhibits low crystallinity characteristics of lacustrine clay authigenesis and is commonly found to fill the interstices among volcanic minerals or envelop them; Li is mainly hosted by Mg-smectite rather than the volcanic minerals. Within the tuffaceous sediment samples, the volcanic glass has undergone a transformation, resulting in its complete disappearance and alteration into clay minerals. Owing to the octahedral sites of Mg-smectite bounded in Li, it is referred to be hectorite. We interpret that the hectorite's precipitation occurs in a high saline-alkaline water environment, a result of McDermitt tuff dissolution. This conclusion can be supported by the coexistence of spherulitic calcite and hectorite. Overall, this study confirms hectorite as the main Li-bearing mineral and increases the understanding of the genetic model of hectorite formation in intracontinental caldera basins.

Keywords McDermitt caldera · Lithium occurrence · Tuffaceous sediments · Mineralogy · Hectorite neoformation

✉ Hanjie Wen
wenhanjie@vip.gyig.ac.cn

1 School of Earth Sciences, East China University of Technology, Nanchang 330013, China

2 State Key Laboratory of Nuclear Resources and Environment, East China University of Technology, Nanchang 330013, China

3 School of Earth Sciences and Resources, Chang'an University, Xi'an 710054, China

4 College of Earth and Planetary Sciences, University of Chinese Academy of Sciences, Beijing 100049, China

5 State Key Laboratory of Ore Deposit Geochemistry, Institute of Geochemistry, Chinese Academy of Sciences, Guiyang 550081, China

6 State Key Laboratory of Environmental Geochemistry, Institute of Geochemistry, Chinese Academy of Sciences, Guiyang 550081, China

1 Introduction

Lithium (Li), a rare metallic element, is distinguished as a crucial energy metal characterized by its high electrochemical potential and low density. Lithium-ion batteries, employing this element, function as high-density energy storage systems for electric vehicles and as secondary storage media for renewable energy sources like solar and wind, thus contributing to curb carbon emissions (Junne et al. 2020; Tabelin et al. 2021). With the current rate of consumption, the demand for Li is projected to surge tenfold by 2050 (Sovacool et al. 2020), necessitating the processing of all viable Li resources to meet this escalating demand. Lithium resources are predominantly found in hard rock, brines, and clays, with clay-type Li deposits receiving increased focus and development due to their substantial reserves and cost-effective

mining and extracting methods (Benson et al. 2017a, 2023; Castor and Henry 2020).

The clay-type lithium deposit located in McDermitt Caldera, Nevada reserves more than 5.1 Mt Li within its mineralized zone, and represents the largest Li deposit in the United States (Gruber et al. 2011; Kesler et al. 2012; Benson et al. 2023). The discovery of Li mineralization and the establishment of mineralogical zoning in McDermitt caldera can be traced back to studies conducted as early as the 1970s (Glanzman et al. 1978; Rytuba and Glanzman 1978). Additional research into the Li content across various alteration zones and tectonic settings has shown that the enrichment of Li in clays is a result of the diagenetic and low-temperature hydrothermal alteration of tuffaceous sediments, occurring under an undrained system (Glanzman et al. 1978; Langella et al. 2001; Benson et al. 2017a; Castor and Henry 2020). The Li-rich layers can be divided into smectite intervals and illite intervals respectively, based on the main clay phases in sediments (Castor and Henry 2020; Ingraffia 2020; Benson et al. 2023). The Li-bearing illite clays are spatially limited and found exclusively in proximity to several faults related to caldera resurgence (Benson et al. 2023). Conversely, smectite clays, dispersed throughout the caldera, serve as the primary hosts for Li and act as the precursors to illite clays (Castor and Henry 2020; Benson et al. 2023). Due to the elevated concentration of Li, in-situ sensitive high-resolution ion microprobe analysis and genetic studies have been performed on intervals dominated by Li-bearing illite (Benson et al. 2023). Despite the significance of the smectite layers in this deposit, it should be noted that only preliminary research has been conducted on them thus far (Glanzman et al. 1978; Odom 1992; Morissette 2012; Castor and Henry 2020). The occurrence of Li and the genesis of Li-bearing minerals within these intervals remain to be determined. To deepen our understanding of this deposit's genesis and improve the metallogenic model, a comprehensive study into the smectite intervals is imperative.

Employing focused ion beam (FIB), time-of-flight secondary ion mass spectrometry (TOF–SIMS), and transmission electron microscope (TEM), this study analyzed the mineralogy and in-situ elemental distribution in smectite-rich tuffaceous sediments, thus facilitating the direct identification and observation of Li-bearing minerals at micro to nano scales. Moreover, employing Nuclear Magnetic Resonance (NMR), we have investigated the bonding environment of Li, which provides new insights into the occurrence of Li in the Li-bearing minerals.

2 Geological setting

The McDermitt caldera, located on the border between northern Nevada and southeastern Oregon in the United States (Fig. 1), displays an irregular keyhole shape, covering an area of $40 \times (30 - 22)$ km^2 (Fig. 2; Henry et al. 2017). Volcanic activity at the McDermitt caldera was associated with the impingement of the Yellowstone plume into the transitional continental crust at the western margin of the North American craton (Camp et al. 2015; Benson et al. 2017a, 2017b). The North American craton later moved over the relatively stable plume tail, and younger silicic centers emerged to the east, creating a linear volcanic track (Fig. 1; Griffiths and Campbell 1991; Camp and Ross 2004; Coble and Mahood 2012). Plume material preferentially ascended beneath thinner accreted oceanic lithosphere located west and north of the $^{87}Sr/^{86}Sr = 0.704$ isopleth (Camp et al. 2015), resulting in an eruption of effusive Columbia River Basalt Group lavas north of McDermitt caldera (Fig. 1) between ~ 17 and 15 million years (Ma) ago. Mafic underplating and magmatic intrusions caused low degrees of partial melting of the transitional continental crust which lies between the $^{87}Sr/^{86}Sr$ 0.706 and 0.704 isopleths forming peralkaline rhyolitic magma chambers in the upper crust, and contributing to the initial enrichment of Li (Coble and Mahood 2012; Benson et al. 2017a, 2017b, 2023).

The eruption of McDermitt Tuff at ~ 16.39 Ma resulted in the evacuation of approximately 1000 km^3 of Li-rich rhyolitic magma (Benson et al. 2017a, 2023; Henry et al. 2017), which led to the large-scale collapse of landforms and the formation of McDermitt caldera and related caldera lake (Lithium Americas Corporation 2018a; Castor and Henry 2020). Between 16.4 and 15.7 Ma ago, regional pyroclastic eruptions resulted in the deposition of glass-rich tuff within the caldera (Castor and Henry 2020). During this interval, post-collapse magmatic resurgence led to the uplift of intracaldera McDermitt Tuff forming an irregular dome (Montana Mountains) extending northward (Fig. 2; Castor and Henry 2020). Lithium is concentrated in lacustrine tuffaceous sediments which mainly accumulated in the moat between the caldera wall and central dome (Fig. 2). The exposure of tuffaceous sediments in the eastern and southern regions of the caldera is limited due to the overlay of Quaternary sediments (Fig. 2). Clays constitute between 60% and 90% volume of the Li-rich sediments, with the remaining volume being occupied by a variety of other materials, including but not limited to, volcanic ash, sandstones, carbonates, conglomerates, and mafic to felsic lavas (Lithium Americas Corporation 2018b; Castor and Henry 2020; Benson et al. 2023). The dominant Li-bearing clay mineral in claystone throughout the caldera is interpreted as smectite (Castor and Henry 2020; Benson et al. 2023), while Li-illite clays, which are formed through hydrothermal alteration, are exclusively found in proximity to faults related to magmatic resurgence (Benson et al. 2023).

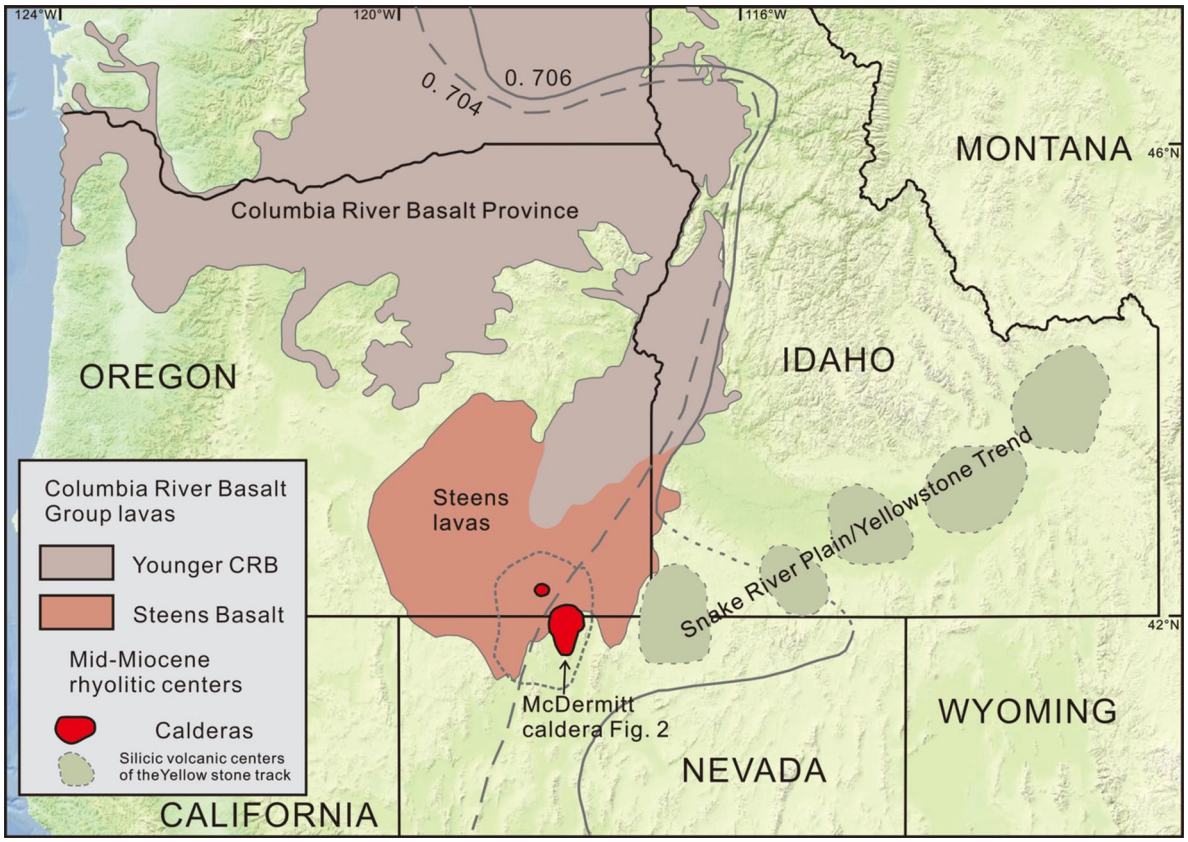

Fig. 1 McDermitt caldera in relation to Yellowstone hotspot track and Columbia River Basalt Province. The location of McDermitt Caldera, Yellowstone hotspot track, and Columbia River Basalt Province, according to Benson and Mahood (2016) and Henry et al. (2017); $^{87}Sr/^{86}Sr_i$ isopleths according to Benson and Mahood (2016)

3 Sampling and analytical methods

3.1 Scanning electron microscope (SEM) analysis

Smectite-rich tuffaceous sediments from McDermitt caldera, northern Nevada, west United States were collected in this study. Representative sample MC-1 with a Li concentration of 1940 ppm was made into a polished thin section for SEM observation. Mineralogy characterization and back-scattered electron (BSE) imagery were performed on the Scios-FIB emission field SEM, equipped with an energy dispersive spectrometer (EDS) at the Institute of Geochemistry, Chinese Academy of Sciences (IGCAS), Guiyang, China. FIB foil was obtained from polished sections using the FEI Scios dual-beam system. Foils were cut from the target area using FIB and mounted on Cu grids.

3.2 TOF–SIMS and TEM analysis

The unthinned foil F1 (Fig. 3d) was used for TOF–SIMS analysis at the National Central for Electron Spectroscopy, Tsinghua University, Beijing, China. The foil then thinned to electron transparency, ideally ~ 100 Å in thickness, and was characterized using the FEI Talos F200X field-emission scanning transmission electron microscope (FE-STEM) operating at 200 kV at the Suzhou Institute of Nano-Tech and Nano-Bionics, Chinese Academy of Sciences.

3.3 Nuclear magnetic resonance (NMR) analysis

The clay-Li coordination environment cannot be directly detected by common synchrotron-based techniques (e.g., X-ray absorption fine structure) and remains an open question. NMR spectroscopy analysis was performed to determine the coordination environment of Li within the host mineral of the sample. Solid-state ^{7}Li NMR experiments were performed on a Bruker Avance III HD 400WB (9.4 T) spectrometer operating at a frequency of 155.2 MHz for ^{7}Li. A WVT double-resonance 4 mm o.d. Bruker cross-polarization magic-angle-spinning (CP-MAS) probe with a spinning frequency of 10.0 kHz was used. The ^{7}Li NMR spectra were recorded with a single pulse excitation using a short pulse length (0.32 µs, with a tip angle of pi/12) to obtain

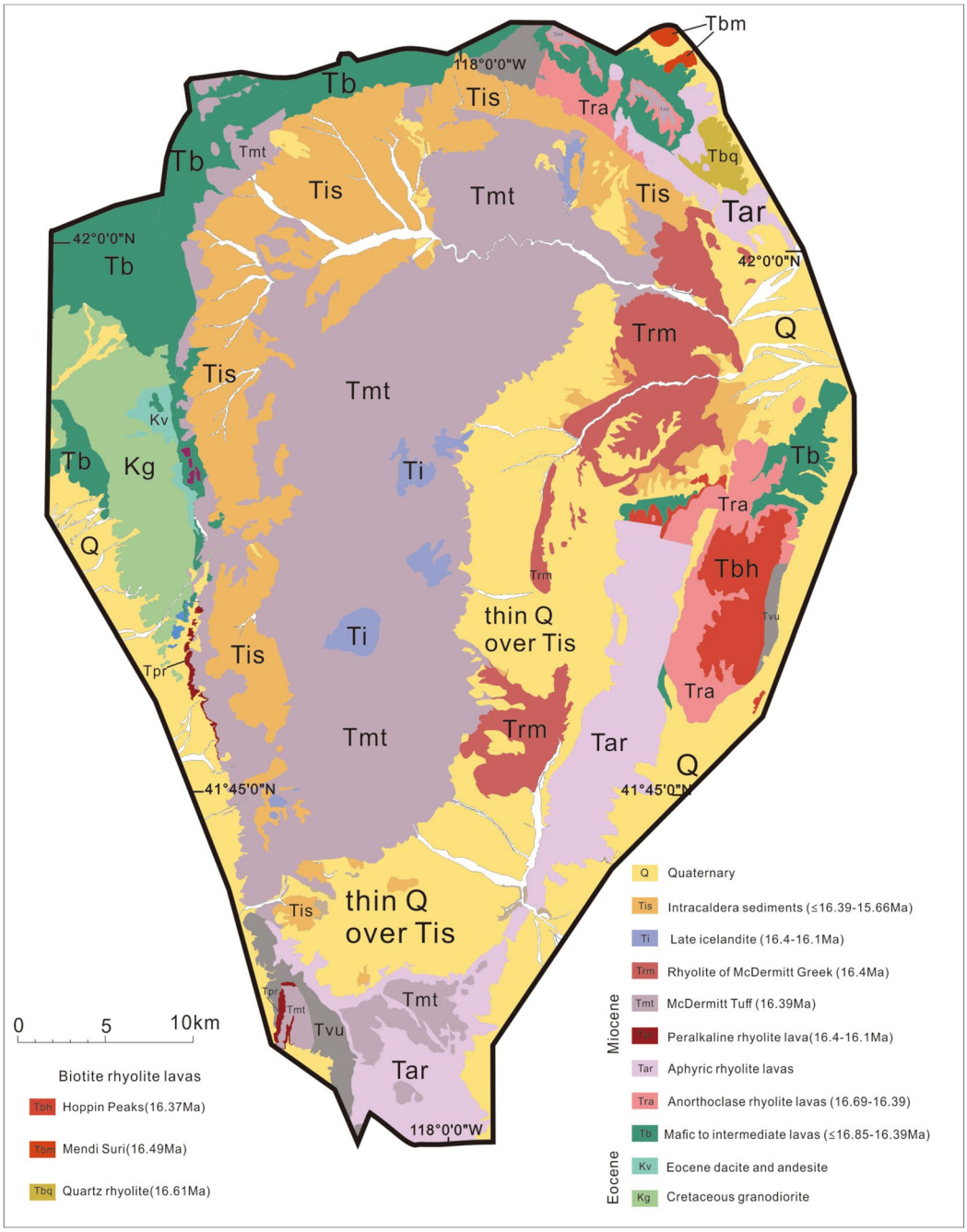

Fig. 2 Simplified geologic map of the McDermitt caldera (after Castor and Henry 2020)

quantitative results and a recycle delay of 1 s. ^{7}Li chemical shifts were referenced using LiCl 1 M in solution as an external reference (0 ppm).

4 Results

4.1 SEM analysis

SEM in backscattered electron (BSE) mode (Fig. 3) and energy dispersive spectrometer (EDS) analysis revealed that the tuffaceous sediment samples comprise volcanogenic crystal fragments, carbonate mineral, and clay mineral, consistent with the XRD results of Castor and Henry (2020)

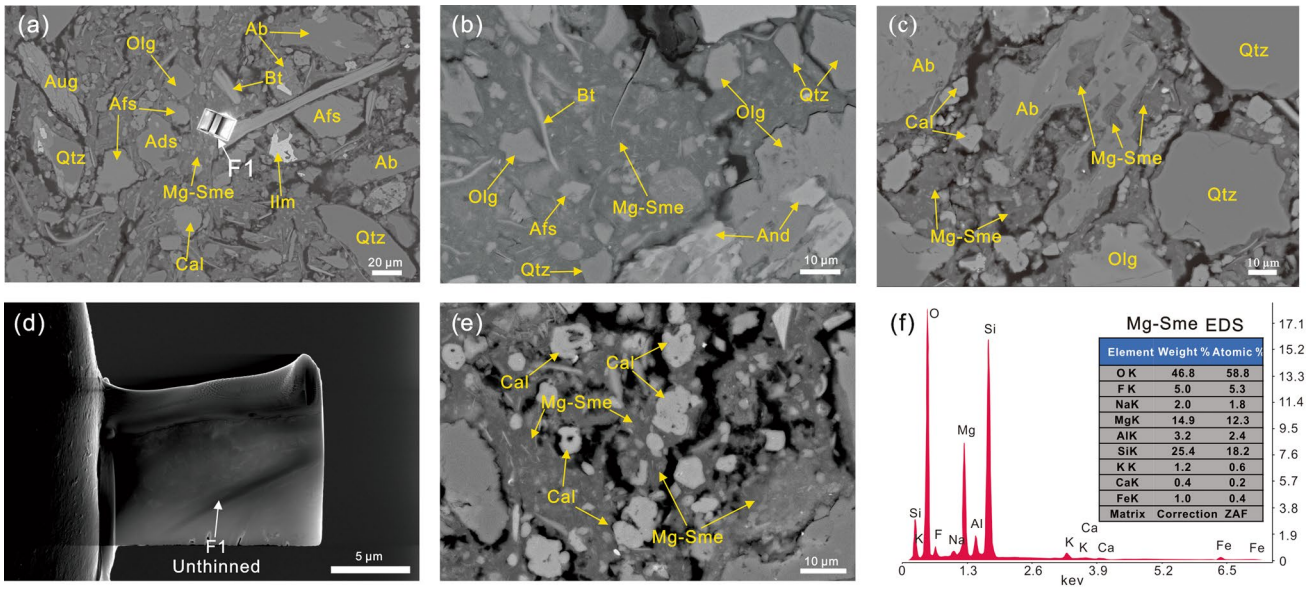

Fig. 3 SEM and EDS analysis of the tuffaceous sediments. **a, b** Volcanogenic minerals, calcite, and the surrounding Mg-smectite. F1 is the FIB excavation site; **c** albite exhibits dissolution edge structures and is filled and coated in-situ by clay minerals; **d** the cross section of F1; **e** Mg-smectite and coexisting spherulitic calcite; **f** EDS spectra for Mg-smectite. Abbreviation: Olg, Olgoclase; Aug, Augite; Ab, Albite; Bt, Biotite; Afs, alkaline feldspar; Ads, Adesine; Ilm, Ilmenite; Qtz, Quartz; And, Andradite; Cal, Calcite; Mg-Sme, Mg-Smectite

and Morissette (2012). Crystal fragments, which include biotite, quartz, hornblende, plagioclase, and alkali feldspar, were observed to display subhedral to angular or polygonal shapes, ranging in size from 20 to 500 μm (Fig. 3a–c). Most of them have smooth and clean surfaces and are dispersed randomly within the matrix without an obvious orientation (Fig. 3a–c). The plagioclase primarily consists of albite, oligoclase, and andesine, with a relatively smaller proportion of alkali feldspar. Some feldspars have been subject to dissolution and are filled and enclosed locally by smectite (Fig. 3c). Biotite was observed to be the dominant femic phase, while amphibole and pyroxene are typically found to be barren. Carbonate minerals, predominantly calcite, are observed to have an uneven spatial distribution (Fig. 3). Notably, some calcite that coexists with clays exhibits a morphology akin to spherulitic calcite (Fig. 3e). Observations under SEM-BSE mode reveal that clay aggregates, which surround the crystal fragments, typically show a darker appearance contrasted with the crystal fragments themselves (Fig. 3). The clay matrix is primarily composed of O, Si, and Mg (Fig. 3f), consistent with magnesian smectite.

4.2 TOF–SIMS analysis

The TOF–SIMS foil (F1) was located within the clay matrix (Fig. 3a). Fig. 4 presents the TOF–SIMS positive secondary ion image for several elements on the FIB cross-section, with intensity color-coded. Black in the images represents areas with no signal or minimal ion presence, while white indicates maximum signal strength and points of maximum ion abundance. The ion corresponding to the intensity distribution map and its MC and TC values are displayed at the bottom left of each image. The short columnar mineral located in the upper right of the cross-section, which is enriched in K, Al, and Si (Fig. 4b, c, g), aligns with the characteristics of alkali feldspar (Fig. 4c). The flaky mineral situated in the lower right, which contains K, Al, Fe, Si, and Mg (Fig. 4a–d, g), aligns with the characteristics of biotite (Fig. 4d). Excluding feldspar and biotite, the primary mineral in the cross-section is a homogeneous phase that is rich in Si and Mg, while virtually devoid of Al (Fig. 4a–c). This observation aligns with the results from the SEM–EDS analysis (Fig. 3f), indicating that it is Mg-smectite. The interlayer cations of Mg-smectite mainly consist of Ca, K, and Na (Fig. 4f–h). The spatial distribution of both Li and Mg-smectite presents a high degree of similarity (Fig. 4a, e). K-feldspar and biotite present in the matrix do not show an enrichment of Li, suggesting that Mg-smectite is the primary carrier of Li.

4.3 TEM analysis

Mg-smectite crystallites, as observed in HRTEM imaging, are characterized by curved lattice fringes and layer terminations, with interlayer spacings that span from 13.3 to 14.7 Å (Fig. 5a, b), which is in good agreement with the prior XRD analysis (Morissette 2012; Castor and Henry 2020). An illite-like phase which may formed by the illitization

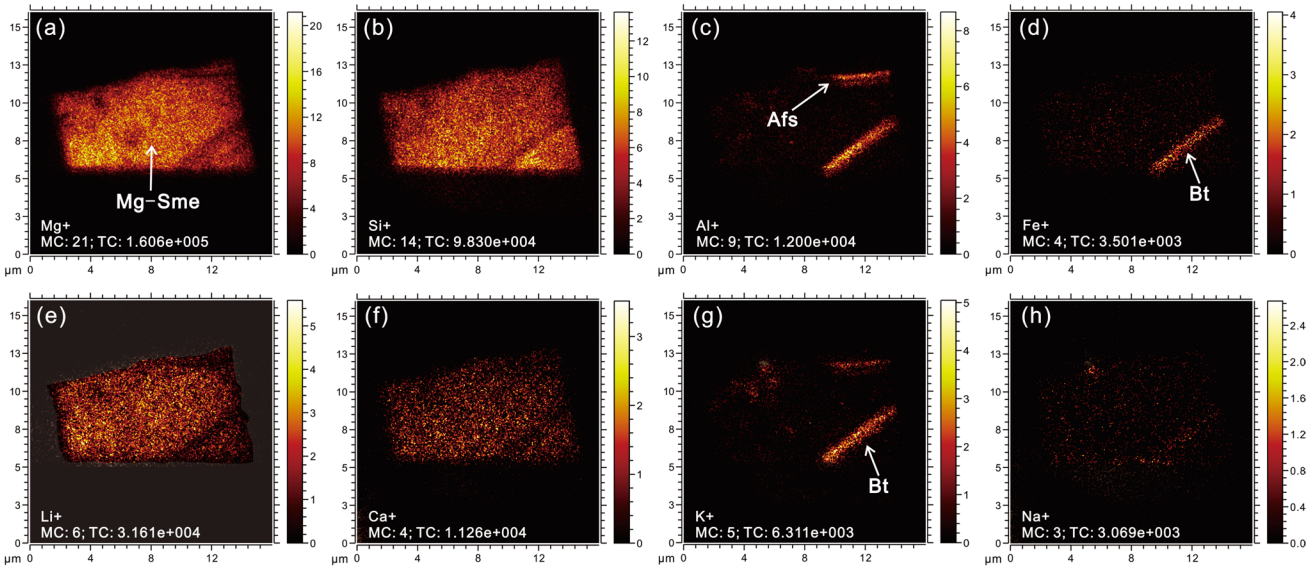

Fig. 4 TOF–SIMS positive secondary ion image collected from F1 for **a** Mg, **b** Si, **c** Al, **d** Fe, **e** Li, **f** Ca, **g** K, **h** Na. Abbreviation: Mc, Maximum counts per pixel; Tc, Total counts of entire image; Mg-Sme, Mg-Smectite; Afs, Alkaline feldspar; Bt, Biotite

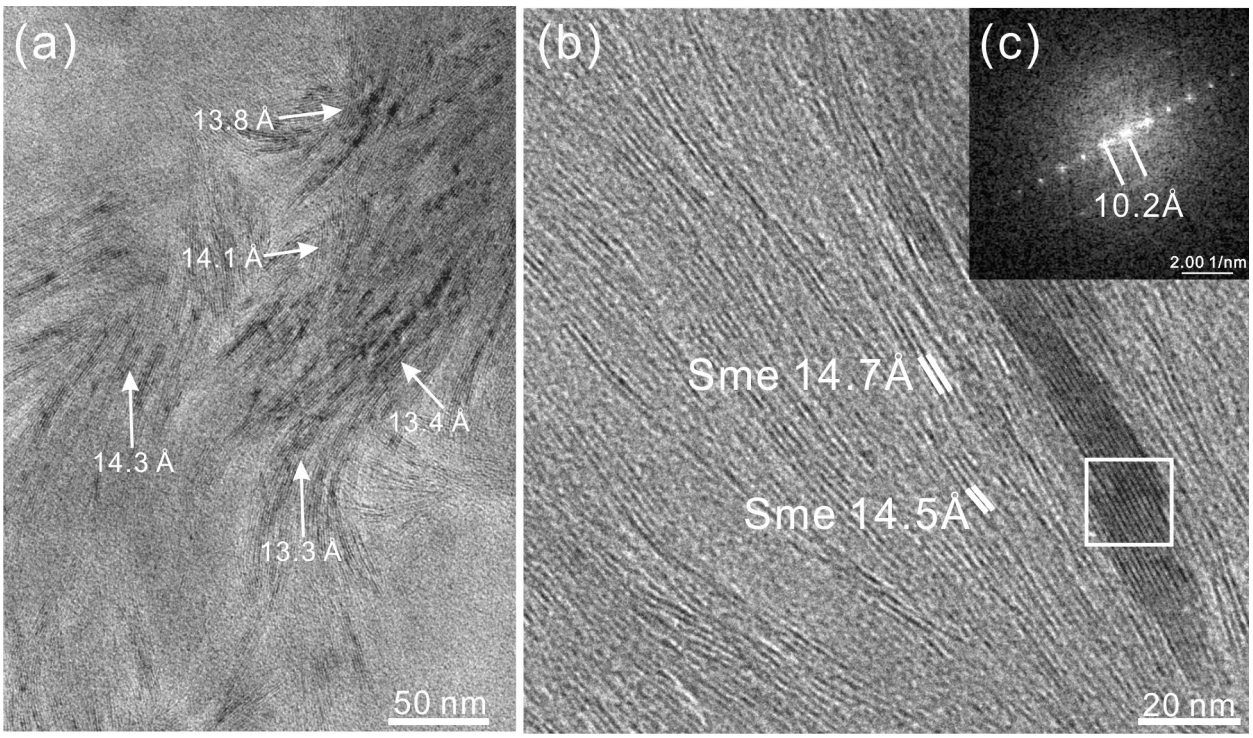

Fig. 5 **a** HRTEM bright-field (BF) images of smectite showing variable fringe spacing; **b** illite-like phase (white rectangular) is surrounded by smectite; **c** FFT image from the white rectangular area reveals an illite-like layer spacing of approximately 10.2 Å

of smectite was found within the smectite matrix (Fig. 5b; white rectangle), characterised by relatively straight layers and lattice spacings of ~ 10.2 Å, as determined by fast Fourier transform analysis (Fig. 5c).

4.4 NMR analysis

In this study, ^{7}Li-NMR analysis is performed to clarify the bonding environment of Li. ^{6}Li and ^{7}Li have the same

chemical shift in identical environments, which mainly depends on the coordination number. The experiment revealed a single peak in the ^{7}Li-NMR spectrum of sample MC-1, exhibiting a chemical shift of − 1.1 ppm (Fig. 6). This result indicates that Li in the sample has a single predominant bonding environment.

5 Discussion

5.1 Lithium's host minerals and bonding environment

Due to its moderately incompatible behavior, Li prefers to remain in the residual melt during magmatic differentiation (Neukampf et al. 2019). A rapidly cooling process can induce the Li-rich melt to crystallize to form fine-grained minerals or quench to form volcanic glass (Černý et al. 2005; Ellis et al. 2022). In the present research, no fresh glass shards were detected using SEM, and the in-situ TOF–SIMS analysis revealed that magmatic fine-grained minerals such as biotite and feldspar demonstrate a low Li concentration (Figs. 3a–c, e and 4c–e, g). The Mg-rich clay matrix is recognized as the primary carrier for Li (Fig. 4a, e).

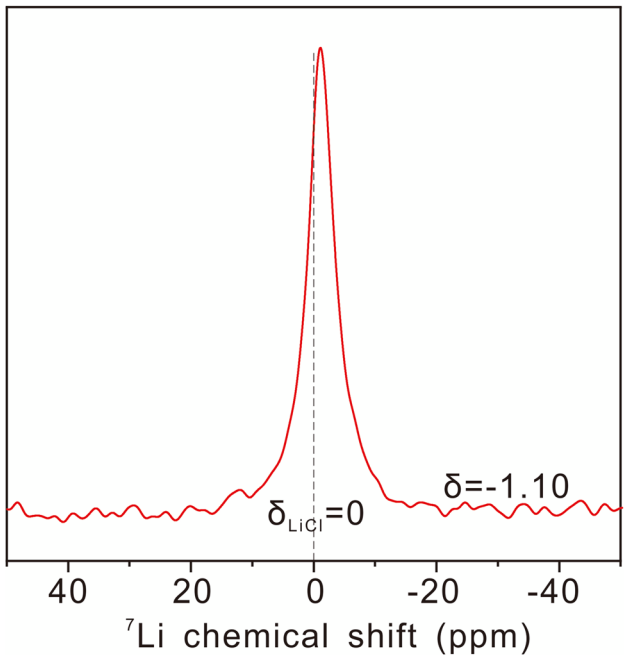

Fig. 6 ^{7}Li-NMR spectra of tuffaceous sediments enriched with Mg-smectite

As depicted in the given figure (Fig. 7), in Mg-smectite, Li (a) likely substitutes for Mg in octahedral sites, exhibiting a coordination number of 6; (b) is adsorbed as bidentate inner-sphere complexes on the edge and basal surface sites, with a coordination number of 4; (c) is absorbed as outer-sphere complexes in interlayer sites, also with a coordination number of 4; (d) is located in pseudo-hexagonal sites, with a coordination number of 6 (Meunier 2005; Kalo et al. 2012; Bauer and Velde 2014; Hindshaw et al. 2019; Borst et al. 2020; Li and Liu 2020; Zhang et al. 2021; Li et al. 2023).

A decrease in coordination number results in reduced electron shielding and a more positive chemical shift (Hindshaw et al. 2019). According to previous experiments, the chemical shift for Li with a coordination number of 4 has a positive ^{7}Li-NMR chemical shift (0–1 ppm), while Li with a coordination number of 6 has a negative chemical shift (− 0.3 to − 1.3 ppm; Xu and Stebbins 1995). The ^{7}Li-NMR results of laboratory-synthesized Mg-rich phyllosilicate show that the pseudo-hexagonal Li displays a chemical shift close to 0 (approximately − 0.1 to − 0.2 ppm). Our experiment results indicate that the ^{7}Li-NMR chemical shift of the Mg-smectite rich sample is − 1.10 ppm (Fig. 6), which falls within the range of chemical shifts observed for 6-coordinated Li (− 0.3 to − 1.3 ppm; Xu and Stebbins 1995). In addition, the structural charge of Mg-smectite, originating in the internal octahedral site and distanced from the clay surface, is not favorable for the formation of pseudo-hexagonal 6-coordinated Li (Bauer and Velde 2014). Therefore, the chemical shift of 6-coordinated Li observed in the ^{7}Li-NMR spectrum is mainly attributed to Li in octahedral sites of the Mg-smectite indicating that the Mg-smectite under study is actually hectorite.

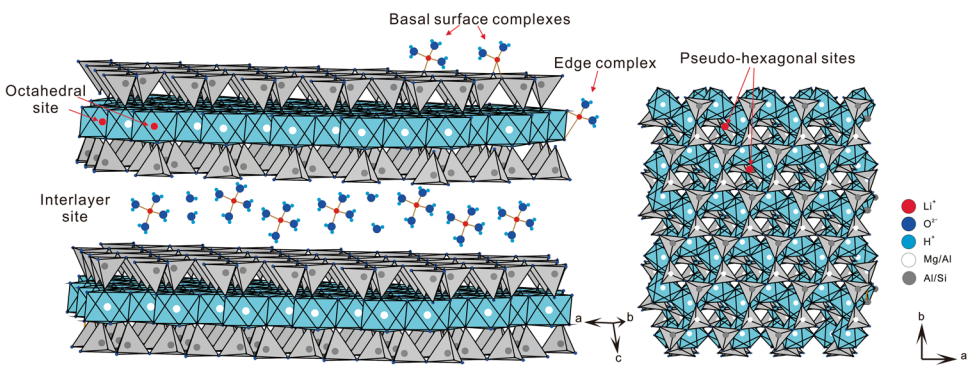

Fig. 7 Schematic figure of the overall structure of a 2:1 type clay mineral shown from two different perspectives and potential lithium binding sites

5.2 The source of Li and the mineralization environment

Previous research has established the McDermitt tuff as a significant Li repository (Benson et al. 2017a; Castor and Henry 2020). Prior to the tuff eruption, the magma exhibited high initial concentrations of Li, which can be attributed to the assimilation of a segment of the felsic continental crust (Benson et al. 2017a). Li present in tuff glass is more susceptible to weathering and potential loss processes compared to other crystalline phases where it is structurally bound within minerals (Ellis et al. 2022). Li presents similar behavior to Na during glass hydration, being rapidly released into the coexisting water (Cuadros et al. 2013a; Ellis et al. 2022). Furthermore, as the intracaldera ignimbrite undergoes cooling, surface degassing may contribute a certain amount of Li to the related hydrologic system (Hofstra et al. 2013; Ellis et al. 2018, 2022).

The McDermitt caldera functioned as an evaporative, siliceous undrained basin (Castor and Henry 2020). The lacustrine setting within this basin exhibited elevated salinity and pH levels, a characteristic supported by the coexistence of autogenetic carbonate and smectite (Fig. 3e; Darragi and Tardy 1987; Hover and Ashley 2003; Furquim et al. 2008; Castor and Henry 2020). The evolution of water chemical composition in such a closed system can be attributed to normal evaporative processes and/or hydrolysis of crystalline and volcanic glass present in the sediments (Langella et al. 2001). Through the hydration of volcanic glass and mineral fragments, an interdiffusion process is initiated. This process involves the outward diffusion of alkaline and alkaline earth cations, while H^+ ions diffuse inward (e.g., volcanic glass $+ H^+ =$ altered glass $+ Na^+ + K^+ + OH^-$; Fig. 8a, Langella et al. 2001; McHenry 2009). This process of ion exchange, in conjunction with evaporation within the hydrologically closed basin, leads the lake water or pore water towards a saline–alkaline condition (Fiore et al. 1999; Langella et al. 2001; McHenry 2009; Deocampo and Jones 2014; Parruzot et al. 2015).

5.3 The formation of hectorite

The genesis of clay minerals in non-tuffaceous sedimentary rocks is complex, with both authigenic and detrital origins. In contrast, volcanic ash lacks clay minerals, rendering the genesis of clay minerals comparatively straightforward. These clay minerals in tuffaceous sediments are typically formed through transformation of volcanic glass (Hong et al. 2019a, 2019b; Yang et al. 2023). When deposited in surface environments, thermodynamically unstable glass shards undergo rapid transformation into clays within a span of hours, days, or years (Berry 1999; Hong et al. 2017, 2019a), leading to the extensive absence of volcanic glass in the tuffaceous sediments.

The HRTEM images of hectorite in this study are consistent with lacustrine clay authigenesis, which tends to produce clay minerals with relatively low crystallinity (Fig. 5; Deocampo et al. 2009, 2010). The depositional environment controls the type of lacustrine autogenetic clays formed through glass transformation (Hong et al. 2017, 2019a). In acidic and freshwater environments with low ionic activity, such as coal-bearing swamps or shallow

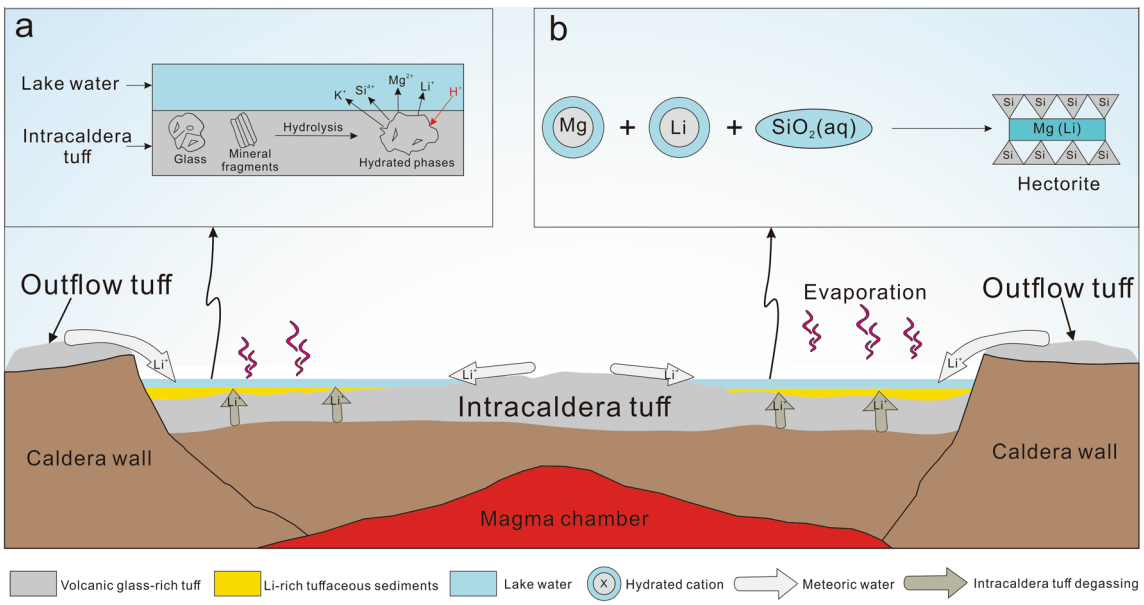

Fig. 8 Schematic model for the formation of McDermitt caldera-hosted Li-rich tuffaceous sediments

lakes, the alteration of volcanic glass to kaolinite occurs (Spears 2012; Pellenard et al. 2017). By contrast, volcanic glass typically transforms into smectites in alkaline environments with relatively high ionic activity (as would be expected in the McDermitt paleo-lake; Huff 2016; Spears 2012).

Volcanic glass transforms into smectites via two models: (1) dissolution and reprecipitation, and (2) in-situ solid-state transformation (Fiore et al. 2001; Cuadros et al. 2013a, 2013b). The intracaldera tuff, primarily rhyolitic, has glass constituents with a high Al/Mg ratio (Le Maitre 1976; Kawano and Tomita 2001; Mandeville et al. 2002; Henry et al. 2017). Should autogenetic smectites originate from the in-situ transformation of volcanic glass, they would be inclined to incorporate Al into their octahedral sites, leading to the genesis of dioctahedral smectites (Cuadros et al. 2013a, 2013b). In fact, under elevated pH (e.g., pH = 9), trioctahedral smectite genesis is possible via a dissolution–precipitation mechanism acting upon volcanic glass with a low concentration of Mg (Cuadros et al. 2013a, 2013b). Consequently, the genesis of hectorite (trioctahedral smectite), within tuffaceous sediments is better explained by the dissolution-reprecipitation model.

The process of magnesian smectites precipitating in solution is predominantly governed by the ion activity of Mg and Si, along with the pH value (Deocampo 2015; Pozo and Calvo 2018). Rhyolitic volcanic rocks typically display low MgO content, ranging from 0.4% to 1.8% (Le Maitre 1976). The incorporation of Mg into clay minerals within rhyolitic ash beds is predominantly attributed to sediment pore waters (Arslan et al. 2010). During the sedimentary process, Mg and Si can diffuse into pore waters through the dissolution of volcanic glass and volcanogenic crystal fragments (e.g., biotite and feldspar) present in tuffaceous sediments (Fig. 8a; Capelli et al. 2021). As evaporation and leaching proceed, there is a corresponding progressive increase in the concentration of Li, Mg, and Si, along with the salinity and alkalinity of the pore waters within the sediments. Calcium carbonate is typically the mineral that first reaches the threshold of solubility (Deocampo and Jones 2014). In contrast, Mg^{2+} ions have a higher kinetic barrier to overcome dehydration of their surrounding hydration sphere and form carbonate minerals, thus making precipitation less likely (Deocampo 2015). Once the silicates precipitate, therefore, they are precipitating in an Mg and Li-enriched aqueous environment, leading to the neoformation of hectorite (Fig. 8b). It's worth mentioning that the occurrence of illitization within the matrix (Fig. 5b) is presumably a result of the interaction between pre-existing smectite and the remaining K-rich brines, contrasting with the thermally induced illitization associated with burial diagenesis.

6 Conclusions

1) The smectite intervals, found in the Li-rich tuffaceous sediments within the McDermitt caldera predominantly consist of clay minerals, volcanic minerals and carbonate. The clay minerals are observed to either fill interstitial spaces between volcanic minerals or envelop them.
2) The primary mineral hosting Li is identified as Mg-smectite in the examined intervals. Li, exhibiting 6-coordination and structural binding in the octahedral sites of Mg-smectite, implies that the Mg-smectite is essentially hectorite.
3) The hectorite was precipitated from lake waters or pore fluids characterized by high salinity and pH which can be supported by the coexisting spherulitic calcite.
4) A lack of volcanic glass in the samples indicates its complete transformation into clays. The high Mg/Al ratio observed in the hectorite suggests that the hectorite genesis occurs via a dissolution–precipitation process.

Acknowledgements This work was financially supported by the National Natural Science Foundation of China (Grant Nos. 92162214, 41773015, and U1812402) and the Key Research and Development Program of Yunnan Province (202103AQ100003).

Author contributions YC, HW, ZZ, and LX—mineralogical, TOF–SIMS, and SEM analyses; SL—TEM analysis; YC, HW, ZZ, KL, and LX—writing of the manuscript.

Declarations

Conflict of interest We declare no conflict of interest in this study.

Ethical approval All authors have approved the manuscript and agree with its submission.

References

Arslan M, Abdioğlu E, Kadir S (2010) Mineralogy, geochemistry, and origin of bentonite in upper Cretaceous pyroclastic units of the Tirebolu Area, Giresun northeast Turkey. Clays Clay Miner. 58(1):120–141. https://doi.org/10.1346/CCMN.2010.0580112

Bauer A, Velde BD (2014) Geochemistry at the Earth's surface: movement of chemical elements. Springer, Berlin, pp 68–71

Benson TR, Mahood GA (2016) Geology of the Mid-Miocene Rooster Comb Caldera and Lake Owyhee Volcanic Field, eastern Oregon: Silicic volcanism associated with Grande Ronde flood basalt. J Volcanol Geotherm Res 309:96–117. https://doi.org/10.1016/j.jvolgeores.2015.11.011

Benson TR, Coble MA, Rytuba JJ, Mahood GA (2017a) Lithium enrichment in intracontinental rhyolite magmas leads to Li deposits in caldera basins. Nat Commun. 8(1):270. https://doi.org/10.1038/s41467-017-00234-y

Benson TR, Mahood GA, Grove M (2017b) Geology and $^{40}Ar/^{39}Ar$ geochronology of the middle Miocene McDermitt volcanic field,

Oregon and Nevada: Slicic volcanism associated with propagating flood basalt dikes at initiation of the Yellowstone hotspot. GSA Bull. 129(9–10):1027–1051. https://doi.org/10.1130/B31642.1

Benson TR, Coble MA, Dilles JH (2023) Hydrothermal enrichment of lithium in intracaldera illite-bearing claystones. Sci Adv. 9(35):eadh8183. https://doi.org/10.1126/sciadv.adh8183

Berry RW (1999) Eocene and Oligocene Otay-Type waxy bentonites of San Diego County and Baja California: Chemistry, mineralogy, petrology and plate tectonic implications. Clays Clay Miner. 47(1):70–83. https://doi.org/10.1346/CCMN.1999.0470108

Borst AM, Smith MP, Finch AA, Estrade G, Villanova-de-Benavent C, Nason P, Marquis E, Horsburgh NJ, Goodenough KM, Xu C, Kynický J, Geraki K (2020) Adsorption of rare earth elements in regolith-hosted clay deposits. Nat Commun. 11:4386. https://doi.org/10.1038/s41467-020-17801-5

Camp VE, Ross ME (2004) Mantle dynamics and genesis of mafic magmatism in the intermontane Pacific Northwest. J Geophys Res. 109(B8):1–14. https://doi.org/10.1029/2003JB002838

Camp VE, Pierce KL, Morgan LA (2015) Yellowstone plume trigger for basin and range extension, and coeval emplacement of the Nevada-Columbia basin magmatic belt. Geosphere. 11(2):203–225. https://doi.org/10.1130/GES01051.1

Capelli IA, Scasso RA, Cravero F, Kietzmann DA, Vallejo D, Adatte T (2021) Late-diagenetic clay mineral assemblages in carbonatized ash beds of the Vaca Muerta Formation (Neuquén Basin, Argentina): Insights into the diagenetic formation of chlorite. Mar Petrol Geol. 132:105207. https://doi.org/10.1016/j.marpetgeo.2021.105207

Castor SB, Henry CD (2020) Lithium-Rich claystone in the McDermitt caldera, Nevada, USA: Geologic, mineralogical, and geochemical characteristics and possible origin. Minerals. 10(1):68. https://doi.org/10.3390/min10010068

Černý P, Blevin PL, Cuney M, London D (2005) Granite-related ore deposits. In: Hedenquist JW, Thompson JFH, Goldfarb RJ, Richards JP (eds) One Hundredth Anniversary Volume. Society of Economic Geologists, Littleton, pp 337–370.

Coble MA, Mahood GA (2012) Initial impingement of the Yellowstone plume located by widespread silicic volcanism contemporaneous with Columbia River flood basalts. Geology. 40(7):655–658. https://doi.org/10.1130/G32692.1

Cuadros J, Afsin B, Jadubansa P, Ardakani M, Ascaso C, Wierzchos J (2013a) Microbial and inorganic control on the composition of clay from volcanic glass alteration experiments. Am Mineral. 98(2–3):319–334. https://doi.org/10.2138/am.2013.4272

Cuadros J, Afsin B, Jadubansa P, Ardakani M, Ascaso C, Wierzchos J (2013b) Pathways of volcanic glass alteration in laboratory experiments through inorganic and microbially-mediated processes. Clay Miner. 48(3):423–445. https://doi.org/10.1180/claymin.2013.048.3.01

Darragi F, Tardy Y (1987) Authigenic trioctahedral smectites controlling pH, alkalinity, silica and magnesium concentrations in alkaline lakes. Chem Geol. 63(1–2):59–72. https://doi.org/10.1016/0009-2541(87)90074-X

Deocampo DM (2015) Authigenic clay minerals in lacustrine mudstones. Larsen D, Egenhoff SO, Fishman NS (eds) Paying Attention to Mudrocks: priceless! Geol Soc Am Spec Pap. 515, Colorado, pp 49–64. https://doi.org/10.1130/2015.2515(03)

Deocampo DM, Jones BF (2014) Geochemistry of saline lakes. In: Holland HD, Turekian KK (eds) Treatise on geochemistry. pp 437–469. https://doi.org/10.1016/B978-0-08-095975-7.00515-5

Deocampo DM, Cuadros J, Wing-dudek T, Olives J, Amouric M (2009) Saline lake diagenesis as revealed by coupled mineralogy and geochemistry of multiple ultrafine clay phases: Pliocene Olduvai Gorge. Tanzania Am J Sci. 309(9):834–868. https://doi.org/10.2475/09.2009.03

Deocampo DM, Behrensmeyer AK, Potts R (2010) Ultrafine clay minerals of the Pleistocene Olorgesailie formation, southern Kenya rift: Diagenesis and paleoenvironments of early hominins. Clays Clay Miner. 58(3):294–310. https://doi.org/10.1346/CCMN.2010.0580301

Ellis BS, Szymanowski D, Magna T, Neukampf J, Dohmen R, Bachmann O, Ulmer P, Guillong M (2018) Post-eruptive mobility of lithium in volcanic rocks. Nat Commun. 9(1):3228. https://doi.org/10.1038/s41467-018-05688-2

Ellis BS, Szymanowski D, Harris C, Tollan PME, Neukampf J, Guillong M, Cortes-Calderon EA, Bachmann O (2022) Evaluating the potential of rhyolitic glass as a lithium source for brine deposits. Econ Geol. 117(1):91–105. https://doi.org/10.5382/econgeo.4866

Fiore S, Huertas FJ, Tazaki K, Huertas F, Linares J (1999) A low temperature experimental alteration of a rhyolitic obsidian. Eur J Mineral. 11:455–470. https://doi.org/10.1127/ejm/11/3/0455

Fiore S, Huertas FJ, Huertas F, Linares J (2001) Smectite formation in rhyolitic obsidian as inferred by microscopic (SEM-TEM-AEM) investigation. Clay Miner. 36(4):489–500. https://doi.org/10.1180/0009855013640004

Furquim SAC, Graham RC, Barbiero L, De Queiroz Neto JP, Vallès V (2008) Mineralogy and genesis of smectites in an alkaline-saline environment of pantanal wetland. Brazil Clays Clay Miner. 56(5):579–595. https://doi.org/10.1346/CCMN.2008.0560511

Glanzman RK, McCARTHY JH, Rytuba JJ (1978) Lithium in the McDermitt caldera, Nevada and Oregon. Energy. 3:347–353. https://doi.org/10.1016/0360-5442(78)90031-2

Griffiths RW, Campbell IH (1991) On the dynamics of long-lived plume conduits in the convecting mantle. Earth Planet Sci Lett. 103(1–4):214–227. https://doi.org/10.1016/0012-821X(91)90162-B

Gruber PW, Medina PA, Keoleian GA, Kesler SE, Everson MP, Wallington TJ (2011) Global lithium availability: A constraint for electric vehicles? J Ind Ecol. 15(5):760–775. https://doi.org/10.1111/j.1530-9290.2011.00359.x

Henry CD, Castor SB, Starkel WA, Ellis BS, Wolff JA, Laravie JA, McIntosh WC, Heizler MT (2017) Geology and evolution of the McDermitt caldera, northern Nevada and southeastern Oregon, western USA. Geosphere. 13(4):1066–1112. https://doi.org/10.1130/GES01454.1

Hindshaw RS, Tosca R, Goût TL, Farnan I, Tosca NJ, Tipper ET (2019) Experimental constraints on Li isotope fractionation during clay formation. Geochim Cosmochim Acta. 250:219–237. https://doi.org/10.1016/j.gca.2019.02.015

Hofstra AH, Todorov TI, Mercer CN, Adams DT, Marsh EE (2013) Silicate melt inclusion evidence for extreme pre-eruptive enrichment and post-eruptive depletion of lithium in silicic volcanic rocks of the western United States: implications for the origin of lithium-rich brines. Econ Geol. 108(7):1691–1701. https://doi.org/10.2113/econgeo.108.7.1691

Hong HL, Fang Q, Wang CW, Churchman GJ, Zhao LL, Gong NN, Yin K (2017) Clay mineralogy of altered tephra beds and facies correlation between the Permian-Triassic boundary stratigraphic sets, Guizhou, south China. Appl Clay Sci. 143:10–21. https://doi.org/10.1016/j.clay.2017.03.014

Hong HL, Algeo TJ, Fang Q, Zhao LL, Ji KP, Yin K, Wang CW, Cheng S (2019a) Facies dependence of the mineralogy and geochemistry of altered volcanic ash beds: an example from Permian-Triassic transition strata in southwestern China. Earth-Sci Rev. 190:58–88. https://doi.org/10.1016/j.earscirev.2018.12.007

Hong HL, Zhao LL, Fang Q, Algeo TJ, Wang CW, Yu JX, Gong NN, Yin K, Ji KP (2019b) Volcanic sources and diagenetic alteration of Permian-Triassic boundary K-bentonites in Guizhou Province South China. Palaeogeogr Palaeoclimatol Palaeoecol. 519:141–153. https://doi.org/10.1016/j.palaeo.2018.01.019

Hover VC, Ashley GM (2003) Geochemical signatures of paleodepositional and diagenetic environments: a STEM/AEM study of authigenic clay minerals from an arid rift basin, Olduvai Gorge Tanzania. Clays Clay Miner. 51(3):231–251. https://doi.org/10.1346/CCMN.2003.0510301

Huff WD (2016) K-bentonites: A review. Am Mineral. 101:43–70. https://doi.org/10.2138/am-2016-5339

Ingraffia JT (2020) Lithium at the thacker pass deposit, Humboldt County, Nevada, USA. Dissertation, University of Nevada, Reno.

Junne T, Wulff N, Breyer C, Naegler T (2020) Critical materials in global low-carbon energy scenarios: the case for neodymium, dysprosium, lithium, and cobalt. Energy. 211:118532. https://doi.org/10.1016/j.energy.2020.118532

Kalo H, Milius W, Breu J (2012) Single crystal structure refinement of one- and two-layer hydrates of sodium fluorohectorite. Rsc Adv. 2(2):8452. https://doi.org/10.1039/c2ra20457f

Kawano M, Tomita K (2001) TEM-EDX study of weathered layers on the surface of volcanic glass, bytownite, and hypersthene in volcanic ash from Sakurajima volcano. Japan Am Mineral. 86(3):284–292. https://doi.org/10.2138/am-2001-2-311

Kesler SE, Gruber PW, Medina PA, Keoleian GA, Everson MP, Wallington TJ (2012) Global lithium resources: Relative importance of pegmatite, brine and other deposits. Ore Geol Rev. 48:55–69. https://doi.org/10.1016/j.oregeorev.2012.05.006

Langella A, Cappelletti P, Gennaro RD (2001) Zeolites in closed hydrologic systems. Rev Mineral Geochem. 45(1):235–260. https://doi.org/10.2138/rmg.2001.45.7

Le Maitre RW (1976) The chemical variability of some common igneous rocks. J Petrol. 17(4):589–598. https://doi.org/10.1093/petrology/17.4.589

Li WS, Liu XM (2020) Experimental investigation of lithium isotope fractionation during kaolinite adsorption: Implications for chemical weathering. Geochim Cosmochim Acta. 284:156–172. https://doi.org/10.1016/j.gca.2020.06.025

Li JT, Liu LS, Kang XJ, Li K, Zhang S, Liu QF (2023) Enrichment of lithium in the claystone coal gangue from the Malan mine, Xishan Coalfield, Shanxi Province. Northern Chin Geochem. 83(2):125972. https://doi.org/10.1016/j.chemer.2023.125972

Lithium Americas Corporation (2018a) Independent technical report for the thacker pass project, Humboldt County, Nevada, USA. https://www.miningdataonline.com/reports/Thacker_Pass_TechReport_05172018.pdf

Lithium Americas Corporation (2018b) Technical report on the prefeasibility study for the thacker pass project, Humboldt County, Nevada, USA. https://www.lithiumamericas.com/_resources/pdf/investors/technical-reports/thacker-pass/Technical-Report-Thacker-Pass.pdf

Mandeville CW, Webster JD, Rutherford MJ, Taylor BE, Timbal A, Faure K (2002) Determination of molar absorptivities for infrared absorption bands of H_2O in andesitic glasses. Am Mineral. 87(7):813–821. https://doi.org/10.2138/am-2002-0702

McHenry LJ (2009) Element mobility during zeolitic and argillic alteration of volcanic ash in a closed-basin lacustrine environment: Case study Olduvai Gorge. Tanzania Chem Geol. 265(3–4):540–552. https://doi.org/10.1016/j.chemgeo.2009.05.019

Meunier A (2005) Clays. Springer, Berlin, p 472

Morissette CL (2012) The impact of geological environment on the lithium concentration and structural composition of hectorite clays. Dissertation, University of Nevada, Reno

Neukampf J, Ellis BS, Magna T, Laurent O, Bachmann O (2019) Partitioning and isotopic fractionation of lithium in mineral phases of hot, dry rhyolites: The case of the Mesa Falls Tuff. Yellowstone Chem Geol. 506:175–186. https://doi.org/10.1016/j.chemgeo.2018.12.031

Odom IE (1992) Hectorite deposits in the McDermitt caldera of Nevada. Min Eng. 44(6):586–589.

Parruzot B, Jollivet P, Rébiscoul D, Gin S (2015) Long-term alteration of basaltic glass: Mechanisms and rates. Geochim Cosmochim Acta. 154:28–48. https://doi.org/10.1016/j.gca.2014.12.011

Pellenard P, Gand G, Schmitz M, Galtier J, Broutin J, Stéyer JS (2017) High-precision U-Pb zircon ages for explosive volcanism calibrating the NW European continental Autunian stratotype. Gondwana Res. 51:118–136. https://doi.org/10.1016/j.gr.2017.07.014

Pozo M, Calvo J (2018) An overview of authigenic magnesian clays. Minerals. 8(11):520. https://doi.org/10.3390/min8110520

Rytuba JJ, Glanzman RK. (1978). Relation of mercury, uranium, and lithium deposits to the mcdermitt caldera complex, Nevada-Oregon. Nevada Bureau of Mines and Geology Report 33, Nevada Bureau of Mines and Geology, Nevada, pp 109–117.

Sovacool BK, Ali SH, Bazilian M, Bazilian M, Radley B, Nemery B, Okatz J, Mulvaney D (2020) Sustainable minerals and metals for a low-carbon future. Science. 367(6473):30–33. https://doi.org/10.1126/science.aaz6003

Spears DA (2012) The origin of tonsteins, an overview, and links with seatearths, fireclays and fragmental clay rocks. Int J Coal Geol. 94:22–31. https://doi.org/10.1016/j.coal.2011.09.008

Tabelin CB, Dallas J, Casanova S, Pelech T, Bournival G, Saydam S, Canbulat I (2021) Towards a low-carbon society: a review of lithium resource availability, challenges and innovations in mining, extraction and recycling, and future perspectives. Miner Eng. 163:106743. https://doi.org/10.1016/j.mineng.2020.106743

Xu Z, Stebbins JF (1995) ^{6}Li nuclear magnetic resonance chemical shifts, coordination number and relaxation in crystalline and glassy silicates. Solid State Nucl Mag. 5(1):103–112. https://doi.org/10.1016/0926-2040(95)00026-M

Yang YY, Liu YQ, Šegvić B, Zhou DW, You JY, Jiao X, Meng ZY, Zhao MR (2023) Origin, transport, and diagenesis of tuffs in organic-rich lacustrine mudstone: an example from the lower part of the Middle-Late Triassic Chang 7 Member, Ordos basin (NW China). Appl Clay Sci. 232:106790. https://doi.org/10.1016/j.clay.2022.106790

Zhang X, (Yvon), Saldi GD, Schott J, Bouchez J, Kuessner M, Montouillout V, Henehan M, Gaillardet J, (2021) Experimental constraints on Li isotope fractionation during the interaction between kaolinite and seawater. Geochim Cosmochim Acta. 292:333–347. https://doi.org/10.1016/j.gca.2020.09.029